Electronic Structure of the Carrier System in Small Semiconductor Particles

Sci. Rep. RITU A39 (1993) pp. 27-31
No. 1, December 1993

Electronic Structure of the Carrier System in Small Semiconductor Particles

Takeshi INAOKA
Department of Materials Science and Technology, Faculty of Engineering,
Iwate University, 4-3-5 Ueda, Morioka 020
(Received November 30, 1993)

We clarify characteristics of the electronic structure of the carrier system in small semiconductor particles, and investigate the size dependence of this electronic structure with the doping level fixed. We assume spherical doped semiconductor particles in an insulating medium or in the vacuum, and calculate the carrier density distribution and the effective one-particle potential self-consistently. Irrespective of the particle size, a prominent peak appears right inside the carrier-deficient surface layer in the carrier density profile. With increase of the size, the density oscillation inside the prominent peak becomes less and less conspicuous, which reduced to nearly constant density to tend toward charge neutrality. The remarkable variation of the potential bending with increasing size depends on where the probability density of newly occupied carrier states is concentrated. This potential variation often entails the intersection of two close energy levels with different concentration features in their probability density distribution.
KEYWORDS: LDA calculation, carrier density distribution, effective one-particle potential, size dependence

1. Introduction

As for the electronic structure of small metal particles, it is established that metal clusters become stabilized at shell-closing electron numbers, and that the electronic shell effect emerges in the size dependence of the ionization potential.[1-5] Compared with these intensive studies, the electronic structure of the carrier system in small semiconductor particles is still open to close examination, though there are some theoretical [6] and experimental [7,8] works on coupled modes of carrier plasmons and polar phonons in small semiconductor particles.

The present analysis is concerned with small doped semiconductor particles in an insulating medium or in the vacuum. Carrier states of semiconductor particles significantly differ from electronic states of metal particles in some points. Firstly, the characteristic length of the carrier density variation near the surface (tens of Å or longer) is much longer than the penetration length of carriers into the surrounding medium or the vacuum (one or a few Å), because the kinetic energy of each carrier (tens of meV or less) is much smaller than the barrier potential at the interface with the insulating medium or the work function (several eV). This is in striking contrast with electronic states of metal particles where the penetration is remarkable in the electron density profile near the surface. (see, e.g., Fig. 3 in ref. 1). Secondly, carriers suffer from the effect of the dielectric polarization of the particle background which accommodates carriers. This polarization effect reduces the Coulomb interaction between carriers. In addition, when a carrier approaches the particle surface, it is affected by the image potential which results from the difference between the dielectric constant of the particle background and that of the surrounding medium or the vacuum.

The aim of the present report is to highlight characteristics of the electronic structure of the carrier system in small semiconductor particles [9] and to examine the size dependence of this electronic structure with the doping level fixed. [10] Our objects of calculation are n-type degenerate GaAs particles which are spherical in shape. In n-type compound semiconductors, such as n-GaAs, n-InSb and n-InAs, carriers readily become degenerate with increase of carrier concentration, because an extremely small effective electron mass and a large dielectric constant give a large effective Bohr radius a_B^*, which leads to a small effective carrier density parameter r_S. Each particle consists of the carriers and the spherical background which is dielectric and electrically positive. The ionized donors are assumed to be spread out into a uniform positive charge distribution. In view of the above-mentioned boundary condition for carriers, we assume that the carriers are restrained in the particle by an infinite barrier potential at the particle surface. This infinite barrier assumption was employed to examine carrier states at the flat semiconductor surface [11] or at the flat oxide-semiconductor interface.[12] We calculate the carrier density distribution and the effective one-particle potential self-consistently.

2. Theory

We employ the density-functional theory involving the local density approximation (LDA). The electronic structure of the carrier ground state can be obtained by solving the following equations self-consistently:

$$\left\{-\left(\hbar^2/2m^*\right)\Delta + V_{eff}\left[\boldsymbol{r}; n(\boldsymbol{r})\right]\right\}\psi_i(\boldsymbol{r}) = E_i\psi_i(\boldsymbol{r}), \quad (1)$$

$$n(\boldsymbol{r}) = \sum_{i=1}^{N}|\psi_i(\boldsymbol{r})|^2, \quad (2)$$

where m^*, N, $n(\boldsymbol{r})$, $\psi_i(\boldsymbol{r})$ and E_i signify the effective mass of carrier electrons, the number of carriers, the carrier number density at position $\boldsymbol{r}$, and the Kohn-Sham [13] single-particle eigenfunctions and eigenenergies, respectively. The effective one-particle potential V_{eff} is composed of the electrostatic Hartree potential V_H, the exchange-correlation potential V_{xc}, and the image potential V_{im}:

$$V_H\left[\boldsymbol{r};\, n(\boldsymbol{r})\right] = \frac{e^2}{\varepsilon_0}\int d^3\boldsymbol{r}'\,\frac{n(\boldsymbol{r}') - n^+}{|\boldsymbol{r} - \boldsymbol{r}'|}, \quad (3)$$

$$V_{xc}\left[n(r)\right] = -\frac{e^2}{2\varepsilon_0 a_B^*}\cdot\frac{2}{\pi}\left(\frac{9\pi}{4}\right)^{1/3}\left[\frac{1}{r_s(r)} + 0.0545\ln\left(1+\frac{11.4}{r_s(r)}\right)\right], \quad (4)$$

$$V_{im}(r) = \frac{\varepsilon_0-\varepsilon_m}{2\varepsilon_0}\cdot\frac{e^2}{R}\sum_{k=1}^{\infty}\frac{k+1}{k(\varepsilon_0+\varepsilon_m)+\varepsilon_m}\left(\frac{r}{R}\right)^{2k}. \quad (5)$$

In eqs. (3)-(5), R, ε_0, ε_m, and n^+ denote the radius of the spherical particle, the static dielectric constant of the particle background, the static dielectric constant of the surrounding medium, and the homogeneously spread-out density of ionized donors, respectively. We adopt the spherical polar coordinates, and locate the origin at the center of the particle. The local effective density parameter $r_s(r)$ is defined by

$$a_B^* r_s(r) = \left[3/4\pi n(r)\right]^{1/3}, \quad (6)$$

where a_B^* is the effective Bohr radius. We employ the exchange-correlation potential parametrized by Gunnarsson and Lundqvist.[14]

Our calculation treats the spherically symmetric system. When the effective potential V_{eff} is spherically symmetric, the angular part of each energy eigenfunction is described by a spherical harmonic $Y_{lm}(\theta, \phi)$, and each energy eigenstate is specified by the quantum numbers n, l and m. Here n (=1, 2,$\cdots$) is the radial quantum number which labels the ascending series of energy levels for each l. The energy eigenstates are degenerate with respect to m. If the carriers have a closed-shell configuration, the carrier density distribution becomes spherically symmetric, which leads to a spherical potential V_{eff}. If the carriers take an open-shell configuration, we utilize the manipulation of replacing the squared eigenfunction $|\psi_{nlm}(r)|^2$ by its average over m $(-l \le m \le l)$, in order to make the carrier density distribution spherically symmetric (see eq. (2.17) in ref. 5).

3. Results and Discussion

Figure 1 exhibits the carrier density distribution $n(r)$ and the effective one-particle potential $V_{eff}(r)$ for three sizes of electrically neutral n-type GaAs particles with closed-shell configurations. All of these particles have the same doping level that corresponds to the bulk carrier concentration $n_b = 5\times10^{17}$ cm^{-3}, namely, to the effective carrier density parameter r_s=0.767. The static dielectric constant of the surrounding medium is taken to be ε_m =1 except for the case where the image potential is switched off by setting $\varepsilon_m = \varepsilon_o$.

The carrier density profile for each size is shown by the full curve in each upper panel of Fig. 1 (a)-(c). The horizontal broken line in each panel indicates the density of the uniformly smeared-out ionized donors. The length is scaled by the effective Bohr radius a_B^*=102 Å. The dotted curves with l assigned represent the decomposition of $n(r)$ into l components, and some of these curves involve more than one shell. The dotted curve labeled 'no V_{im}' in Fig. 1 (b) displays the carrier density distribution obtained from the self-consistent calculation in the absence of the image potential. The dotted curve labeled 'film' in Fig. 1 (c) exhibits the carrier density distribution in the film with the same doping level. The thickness of this film is equal to the diameter of the particle. Here the z-axis is taken to be normal to the surface, and its origin is located right in the middle of the film.

The effective one-particle potential and the occupied energy levels for each size are shown by the full curve and the full bars, respectively, in each lower panel of Fig. 1 (a)-(c). The energy of V_{eff} is measured from its value at the center and scaled by the effective Rydberg constant $R_y^*=e^2/2\varepsilon_0 a_B^*$=5.48 meV. In the lower panel of Fig. 1 (a), the effective potential is decomposed into the electrostatic Hartree potential V_H, the exchange-correlation potential V_{xc}, and the image potential V_{im}. In Fig. 1 (b), the dotted curve and bars display the effective potential and the occupied energy levels in the absence of the image potential. In Fig 1 (c), the dotted curve and bars represent the effective potential, the subband bottoms, and the Fermi energy for the film. The plus or minus sign indicates the parity (even or odd) of the eigenfunction for each subband with respect to the reflection operation $z \to -z$.

First, we focus our attention on the carrier density distribution (see the full curve in each upper panel of Fig. 1 (a)-(c)). The value of the carrier density falls and vanishes at the surface, which forms a carrier-deficient surface layer with positive charges. Right inside this surface layer emerges a prominent peak whose magnitude is considerably larger than the uniform donor density. The prominent peak is the pronounced feature in the carrier density profile regardless of the particle size.

The oscillatory pattern of the density profile varies significantly as one shell after another becomes occupied with increase of the size (see Fig. 1 in ref. 10). This variation can be understood by taking account of the following two facts: (1) The probability density distribution of the newly occupied shell creates a corresponding new feature in the density profile. (2) Once a shell is closed, its component in the density profile declines gradually in magnitude with increase of the size, because a fixed number of carriers in the shell spread over the larger region.

With increasing size, the density oscillation inside the prominent peak becomes less and less conspicuous, which reduces to nearly constant density to tend toward charge neutrality.

In Fig. 1(c), the result of the particle calculation is compared with that of the film calculation. The density oscillation in the film is much less conspicuous than that in the particle.

The image potential operates to repel the carrier into the inside of the particle, when it approaches the surface. As shown in the upper panel of Fig. 1(b), if the image potential is switched off, a small fraction of interior carrier charges transfer to the surface region, because carriers can get closer to the surface.

Here we turn our attention to the effective one-particle potential and the occupied energy levels (see the full curve and the full bars in each lower panel of Fig. 1(a)-(c)). The radial dependence of the effective potential

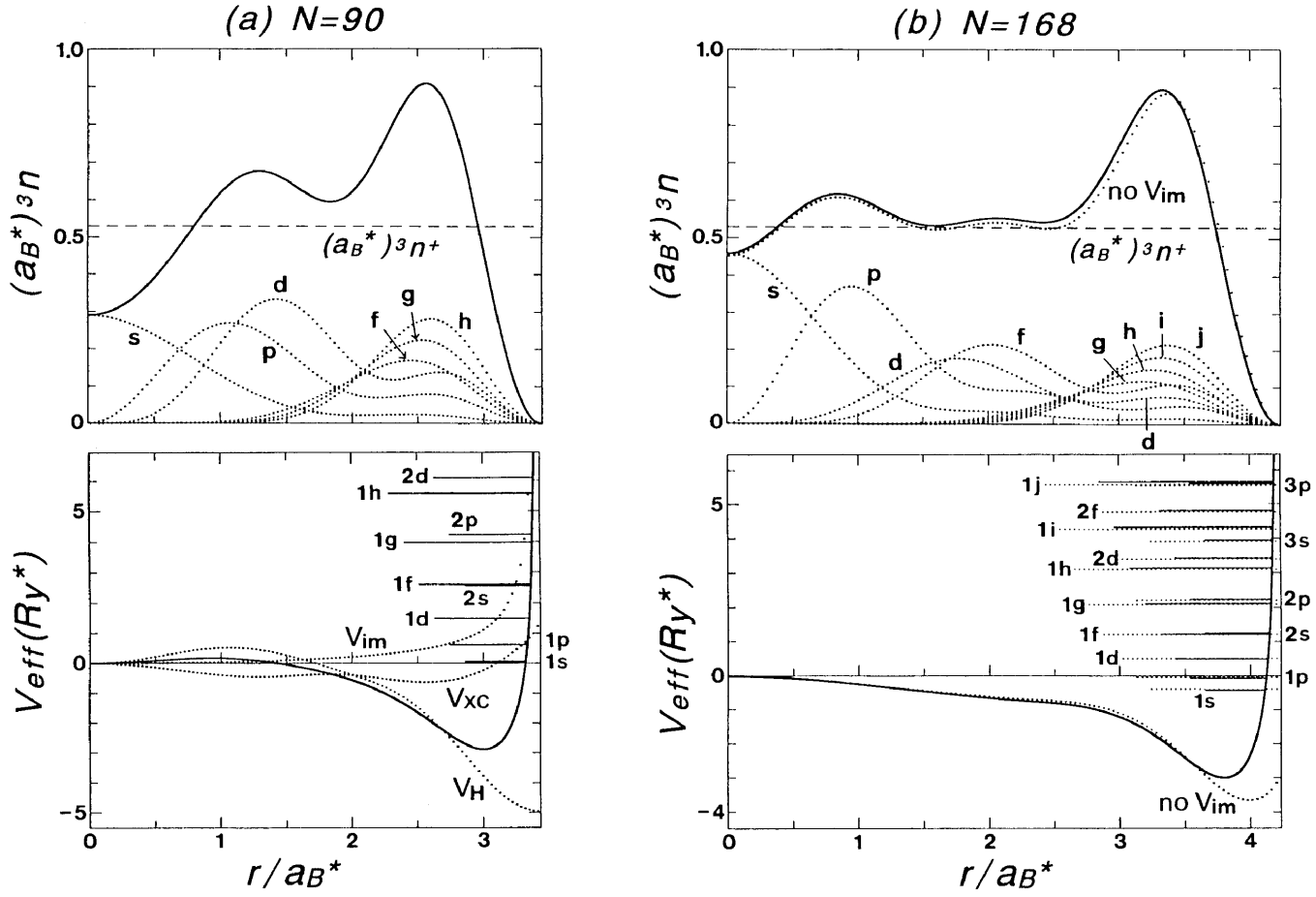

Fig. 1. Electronic structure of the carrier ground state of spherical n-type GaAs particles for three sizes. N denotes the carrier number. Adapted from Fig. 1 in ref. 10. For details, see the text.

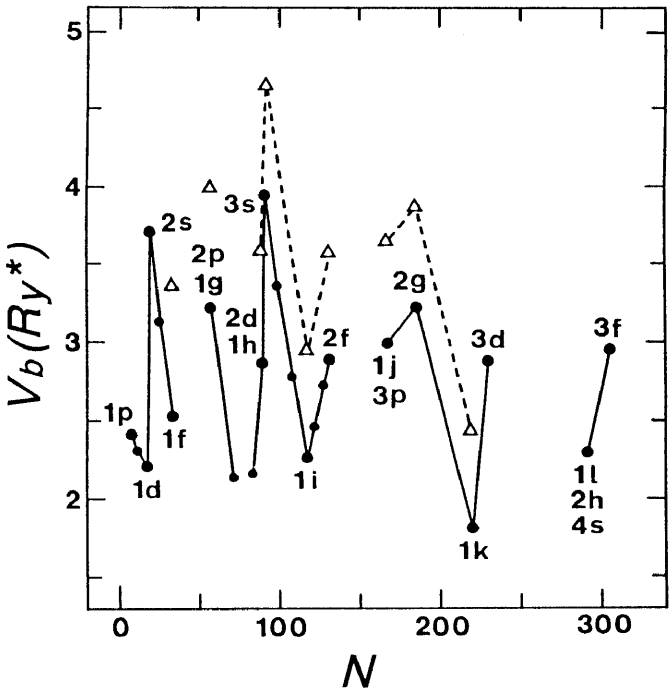

Fig. 2. Size dependence of the magnitude of the downward effective-potential bending in the presence of the image potential (filled circles) and in the absence of the image potential (open triangles). Adapted from Fig. 3 in ref. 10.

is characterized by the downward bending and the quick ascent just near the surface. Figure 2 exhibits the size dependence of the potential bending V_b in the presence of the image potential (filled circles) and in the absence of the image potential (open triangles). The doping level is fixed at the same as in Fig. 1, when the size is changed. The value of V_{eff} is measured from its value at the center, and the potential bending V_b is defined as the absolute value of the minimum of V_{eff}. Larger filled circles and all open triangles correspond to closed-shell configurations, while smaller filled circles correspond to open-shell configurations. The newly occupied shell or shells are specified at each closed-shell point. For example, the 1g and 2p shells are newly filled when the size increases from N=34 to N=58. We can acquire no correct self-consistent solution for closed-shell configurations and their neighboring open-shell configurations in the size ranges where the connecting lines are missing. This difficulty may happen when one of two very close energy levels is occupied and the other is empty. The self-consistent calculation assuming one of the two levels to be occupied and the other to be empty leads to an incorrect solution where the empty level is slightly lower than the occupied level. We meet with the same difficulty in the LDA calculation of the electronic structure of small metal particles.[4] The reason why we encounter this difficulty more often in the present calculation is that, as is described below, the energy-level intersection often occurs with change of the size.

The potential bending varies remarkably with change of the size. Increase (Decrease) of the downward bending lowers (heightens) the energy levels of the shells whose probability density is localized near the surface. Accordingly, the variation of the potential bending often entails the energy-level crossing between the shells with different localization features in the probability density distribution.[10]

The effective potential is decomposed into three components in the lower panel of Fig. 1(a). The downward bending of V_{eff} originates from the downward electrostatic Hartree potential V_H generated by the charge density distribution due to negative carriers and positive donors. The image potential V_{im} operates against the downward Hartree potential to suppress the downward bending of V_{eff} and to make the rapid ascent of V_{eff} in the close proximity of the surface. Switching off the image potential enhances the downward bending of V_{eff}, which leads to an upward rigid shift of the saw-tooth pattern of V_b in Fig. 2. The exchange-correlation potential V_{xc} only plays a subsidiary role, because our carrier system has a small effective density parameter r_s, namely, a high effective density.

The oscillatory variation of V_b in Fig. 2 results from the serial occupation from one shell to another with increase of the size. As is mentioned above, the downward bending of V_{eff} arises from the downward electrostatic Hartree potential V_H. We can decompose V_H into constituent shell components (see Fig. 4 in ref. 10). The (n, l) component of V_H is generated by the charge density distribution $n(r;\ \mathrm{n}l\ ) - n^+(\mathrm{n}l\ )$, where $n(r;\ \mathrm{n}l\ )$ and $n^+(\mathrm{n}l\ )$ denote, respectively, the (n, l) -shell component of the carrier density and the constant component of the homogeneous donor density which cancels with $n(r;\ \mathrm{n}l\ )$ as a whole. A downward electrostatic potential is produced by the carrier density component which is concentrated around the center or well inside the particle. This downward potential operates to enhance the downward bending of V_{eff}. On the other hand, the upward trend is dominant in the electrostatic potential created by the carrier density component which is localized near the surface. This upward tread acts to suppress the downward bending of V_{eff}. From this decomposing analysis, it is established that the value of V_b increases when we are filling a shell whose probability density is concentrated around the center or well inside the particle, and that the value of V_b decreases when we are filling a shell whose probability density is localized near the surface.

4. Summary

Taking account of semiconductor characteristics, we have examined the electronic structure of the carrier ground state of small semiconductor particles. The particles are assumed to be in an insulating medium or in the vacuum. We have performed the self-consistent calculation for various sizes of spherical degenerate semiconductor particles with the doping level fixed.

(1) The carrier density distribution

Irrespective of the size, a prominent peak emerges just inside the carrier-deficient surface layer in the density profile. With increase of the size, the density oscillation inside the prominent peak becomes less and

less conspicuous, which reduces to almost constant density to achieve charge neutrality.

(2) The effective one-particle potential

The magnitude of the downward bending of the effective potential makes a remarkable oscillatory variation with increase of the size. The downward bending tends to increase, when the probability density of the newly filled shell is concentrated around the center or well inside the particle, while it tends to decrease, when the probability density of the newly occupied shell is localized near the surface. This significant variation of the potential bending often involves the intersection of two close energy levels with different angular momenta l.

The present report has been concerned with electrically neutral particles. However, the number of carries may not be balanced with that of ionized donors or acceptors, if our particle system can exchange carriers with its surroundings or surface states. Some analysis of this imbalanced situation is presented in ref. 10.

Acknowledgments

The author is deeply indebted to M. Hasegawa for valuable discussions. He is also grateful to H. Ojima for her help with typing the manuscript. This work is supported by a Grant-in-Aid for Scientific Research from the Ministry of Education, Science and Culture, under No. 04640359. Part of this work was carried out under the Visiting Researcher's Program of the Institute for Materials Research, Tohoku University, through No. 93-143.

1) W. Ekardt: Phys. Rev. B **29** (1984) 1558.
2) D. E. Beck: Solid State Commun. **49** (1984) 381.
3) W. D. Knight, K. Clemenger, W. A. de Heer, W. A. Saunders, M. Y. Chou and M. L. Cohen: Phys. Rev. Lett. **52** (1984) 2141.
4) M. J. Puska, R. M. Nieminen and M. Manninen: Phys. Rev. B **31** (1985) 3486.
5) Y. Ishii, S. Ohnishi and S. Sugano: Phys. Rev. B **33** (1986) 5271.
6) K. S. Srivastava, A. Tandon, M. Trivedi and N. Fatima: Physica B **159** (1989) 295.
7) K. Yamamoto, K. Kimura, M. Ueda, H. Kasahara and T. Okada: J. Phys. C: Solid State Physics. **18** (1985) 2361.
8) Y. Sasaki, Y. Nishina, M. Sato and K. Okamura: Phys. Rev. B **40** (1989) 1762.
9) T. Inaoka: J. Phys.: Condensed Matter **4** (1992) L601.
10) T. Inaoka: J. Phys.: Condensed Matter **5** (1993) 7587.
11) G. A. Baraff and J. A. Appelbaum: Phys. Rev. B **5** (1972) 475.
12) T. Ando: J. Phys. Soc. Jpn **39** (1975) 411.
13) W. Kohn and L. J. Sham: Phys. Rev. **140** (1965) A 1133.
14) O. Gunnarsson and B. I. Lundqvist: Phys. Rev. B **13** (1976) 4274.